CHAPTER 4
RESULTS AND DISCUSSION

In this chapter, the results are presented of the investigation of ZrO_2 reinforced dental porcelain systems. Chemical composition, microstructure properties relationships are brought out and discussed in terms of phase formation, densification and mechanical properties.

4.1 Physical properties

The densification of the ZrO_2-modified porcelain ceramics at various firing schemes is investigated. The change in density versus the tempering time (0-90 min) is shown in Table 4.1. In the tempering time range of 0-30 min, the density increases with increasing tempering time. Further increase in the tempering time to 90 min leads to the decrease of the density. This feature creates a maximum density value of about 2.76 g/cm^3 which is comparable to the values reported by Pisitanusorn et al. (~2.74 g/cm^3 [2]) where whisker-type TiO_2 was used as additive. The increasing density with rising tempering time up to 30 min may be explained by the enhanced densification related to the effect of ZrO_2 and the more reactive two-step sintering used [4, 5, 103]. Further increase in the tempering time causes a decrease in density values. This may be attributed to the suppression of atomic diffusion at probably too long tempering times resulting in an incomplete densification [103]. Similar behavior is also reported by Wang et al. [103] for fine alumina-zirconia ceramics. As is well known, the difference in thermal expansion between the tetragonal leucite crystals and the glassy matrix also provides tangential compressive stresses around the crystals that are thought responsible for significant strengthening in dental porcelain [10, 11]. The crystallization of a high expansion tetragonal leucite phase into a base glass is advantageous to increase its expansion coefficient to a level sufficient to allow efficient bonding to metals [76]. More recently, leucite has been used in all-ceramic materials, not for thermal compatibility, but as a reinforcing material for all-ceramic restorations [10, 11].

To study the crystalline phase development with different firing schemes in each porcelain-based samples, they were heat treated at various condition (Table 4.1), followed by phase analysis using XRD technique. The X-ray diffraction patterns of both unfired and single (one-step) sintered dental porcelain ceramics in this study are given in Fig. 4.1(a and b), indicating a background of amorphous glassy phase and evidence of the formation of only leucite crystalline phase, which could be matched with JCPDS file no. 15-47, in agreement with other works [76, 152]. To a first approximation, this crystalline phase has a tetragonal leucite-type structure in space group $I4_1/a$ (no. 88) with cell parameters $a = 1306$ pm and $c = 1375$ pm [153].

As demonstrated in Fig. 4.1(c-j), it can be seen that all samples showed almost identical XRD patterns. The strongest reflection in the majority of XRD traces derived from all 20 wt% ZrO_2-modified porcelain groups indicated a combination of monoclinic-zirconia which could be match with JCPDS file no. 36-420 [154] and tetragonal-leucite phase. In addition, it should be noted that XRD peaks of leucite (323) and zirconia (111) at $2\theta \sim 28.5°$ are superimposed. In this study, no phase transformation of leucite can be detected at 1040°C and the XRD patterns of the samples subjected to the two-step sintering process for various tempering time from 0 to 90 min did not reveal the formation of any additional crystalline phases, in agree with previous studies [10, 11]. This is probably indicating the effectiveness of ZrO_2 as the leucite stabilizer, in analogous with those found for other similar system [76].

In order to evaluate the relative amounts of tetragonal leucite phase in each group, the leucite peak at the 004 and 400 reflections and the zirconia peak at the 111 reflection were the peaks of interest (Fig. 4.2). As suggested by Ong et al. [152], powder X-ray diffraction method can be used to approximate the amount of leucite phase in porcelain ceramics. From Table 4.1, it can be seen that some relationship was found between the tempering time at 940°C and the concentration of leucite phase in the samples. In this study, the amount of leucite phase in the ZrO_2-doped porcelain specimens subjected to the two-step sintering was found to slightly increase as a function of tempering time, consistent with those reported by Cattell et al. [10, 11] for porcelain-based samples. It has been observed that with increasing tempering time, some diffraction lines gradually sharpen e.g. (004) and (400) peaks, an indication of continuous increase in crystalline size and of the reduction of lattice

Table 4.1 The firing schemes employed for the production of samples and physical properties.

| Materials | Firing condition | | | Density (g/dm^3) | Leucite content $(wt\%)$ | Leucite crystallite size $(\pm 2\ nm)$ | Leucite particle size range $(\pm 30\ nm)$ |
	T_1 Temp. /Dwell time (˚C/min)	T_2 Temp./ Dwell time (˚C/min)	Quenched				
Dental porcelain	980/5	-	-	2.43	-	14.31	200-500
CG	1,040/5	-	-	2.73	26.51	12.53	80-220
G1	1,040/0	-	√	2.72	23.00	9.40	30-93
G2	1,040/1	-	√	2.71	23.80	9.86	37-110
G3	1,040/3	-	√	2.73	24.47	10.04	40-130
G4	1,040/5	-	√	2.72	25.90	10.83	60-130
G5	1,040/5	940/0	√	2.73	25.81	11.93	60-170
G6	1,040/5	940/30	√	2.76	28.40	14.32	60-170
G7	1,040/5	940/60	√	2.71	27.63	16.11	70-180
G8	1,040/5	940/90	√	2.71	30.00	19.90	70-190

58
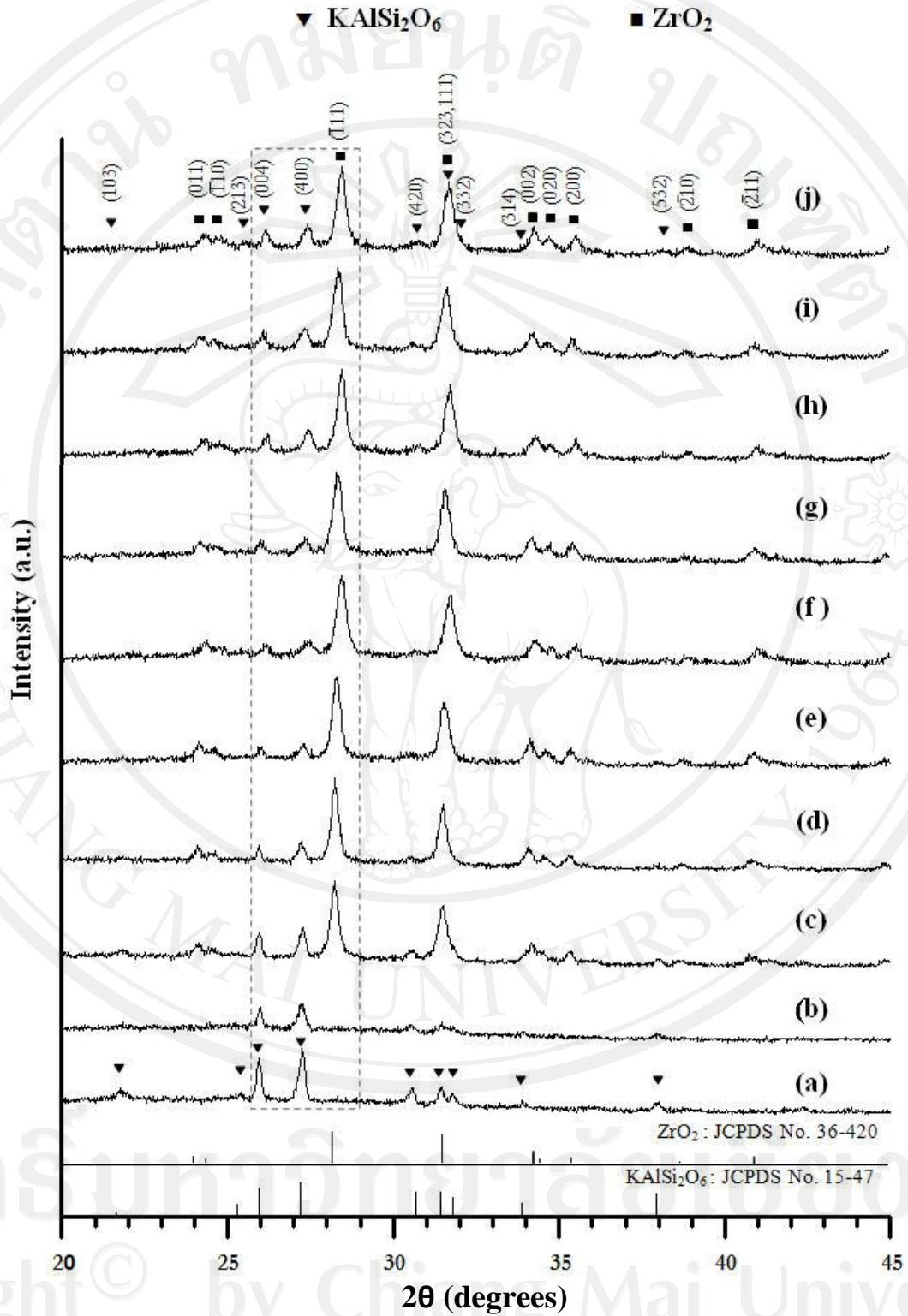
Fig 4.1 X-ray diffraction of patterns of non sintered dental ceramic (a), sintered (b) dental ceramic, non sintered (c) and sintered (d) CG, two-step sintered (e) G3, (f) G4, (g) G5, (h) G6, (i) G7, and (j) G8 samples.
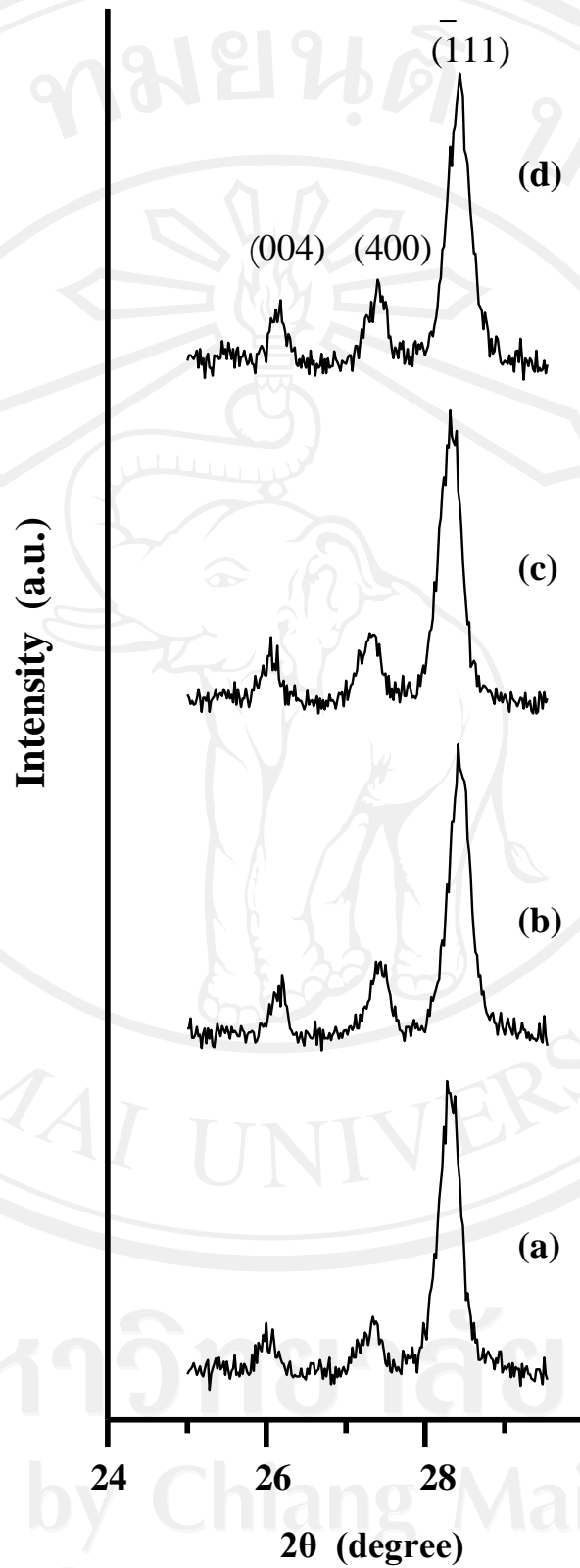
Fig. 4.2 Enlarge X-ray diffraction patterns of (a) G5, (b) G6, (c) G7 and (d) G8 samples.

strain. These observations point out that the prolonged tempering treatment affects the leucite crystallite size.

Additionally, the crystallite size of leucite phase was estimated from these XRD patterns as also given in Table 4.1. The calculated crystallite size value was also found to increase with increasing tempering time. Though, the relative intensities of the Bragg peaks exhibit independent of tempering time, it is well documented that, as Scherer's analysis provides only a measurement of the extension of the coherently diffracting domains, the crystallite sizes determined by this method can be significantly under estimated [144]. In addition to strain, factors such as defects, homogeneity of materials, the complex nature of the background due to amorphous matrix, processing variables and instrument effect can attribute to peak shape, making it almost impossible to extract a reliable crystallite size solely from XRD [144]. In this connection, SEM was also employed for grain size measurement (Table 4.1 and Fig. 4.3).

Microstructural features of dental porcelain ceramics sintered at 1040 ˚C for 5 min are shown in Fig. 4.3(a). It is seen that a smooth surface of typical porcelain glass-ceramics is observed, consistent with those reported earlier [10, 155, 156]. As shown in Fig. 4.3(b-f) for the case of all 20 wt% ZrO_2-modified porcelain ceramics, it can be seen that some leucite particle sizes in the range ~100-300 nm (closer observation of Fig. 4.3(d) as inserted) were initiated from the surface of zirconia grains. It is interesting to noted that dendritic leucite morphology previously reported by several researchers [70, 157] are also found here. These observations may be attributed to the influence of ZrO_2 additives as nucleating agents for leucite crystallization behavior, similar to those found in other similar glass-ceramic systems [70]. The micro-structural evolution for the two-step sintering of the ZrO_2-modified porcelains as a function of tempering time was also revealed, as illustrated in the SEM micrographs (Fig. 4.3(c-f)). All sintered samples showed two (or more) distinct phase structures with a glassy matrix phase reinforcing crystalline phase dispersed in the glassy matrix. In general, they have a very fine microstructure with agglomerates. SEM-EDX analysis of the dental porcelain ceramics marked as "(1)" reveals the strong presence of silica and oxygen indicating the compositional of glass matrix (Fig. 4.4(b)). As shown in Fig. 4.4(a) and (c), EDX spectra obtained from area "(2)"

confirms the existence of all key elements related to the composition of leucite ($KAlSi_2O_6$) [153]. Whilst EDX analysis of the large grain marked as "3" show only zirconia rich phase together with spectra of oxygen, indicating the existence of ZrO_2 additive. The results of SEM-EDX measurement supported the XRD observation discussed earlier (Fig. 4.1 and 4.2). Fig. 4.3(c) is a SEM micrograph of the samples experienced the two-step sintering with no tempering time (i.e. at 0 min) showing leucite particulates which vary between 100 and 300 nm in size and are clustered together along the glassy grains. On the basis of this, the governing mechanism for the appearance of leucite phase in the glassy matrix is surface crystallization [10, 158] Furthermore, there is no evidence of crack formation in the matrix or within the leucite crystals. A similar microstructure was evident for the tempering times 30, 60 and 90 min samples, but with increased leucite growth and signs of ZrO_2 growth, as shown in Fig. 4.3(d-f). In both G7 and G8 samples, the additives are observable in two forms: the agglomerates as also found in G4 and G5, and the nanocomposite formations in reticulate sheets (~100 nm thickness). Such a difference in morphology may be described on the basis of difference in crystallization and growth mechanisms. The early stages of bulk leucite growth have been observed as dendrites growing in their preferred crystallographic directions. A diffusion controlled growth process that evolved at the smooth atomic-scale faceted crystal-glass interface was suggested. With longer tempering times applied, a significant change in dendrite shape due to the growth of secondary and tertiary fibrils and their ripening resulted in a highly organized tetragonal leucite structure, consistent with those observed in other similar systems [2, 158, 159]. Signs of leucite particle coalescence were also visible in all ZrO_2-modified porcelain samples which may have been driven by a reduction in interfacial energy when larger particles grow at the expense of smaller ones (Ostwald ripening) [160]. In this study, it is believed that the prolonged tempering times may have allowed sufficient time for small particles below a critical size to dissolve and feed larger particles via a diffusion down the concentration gradient.
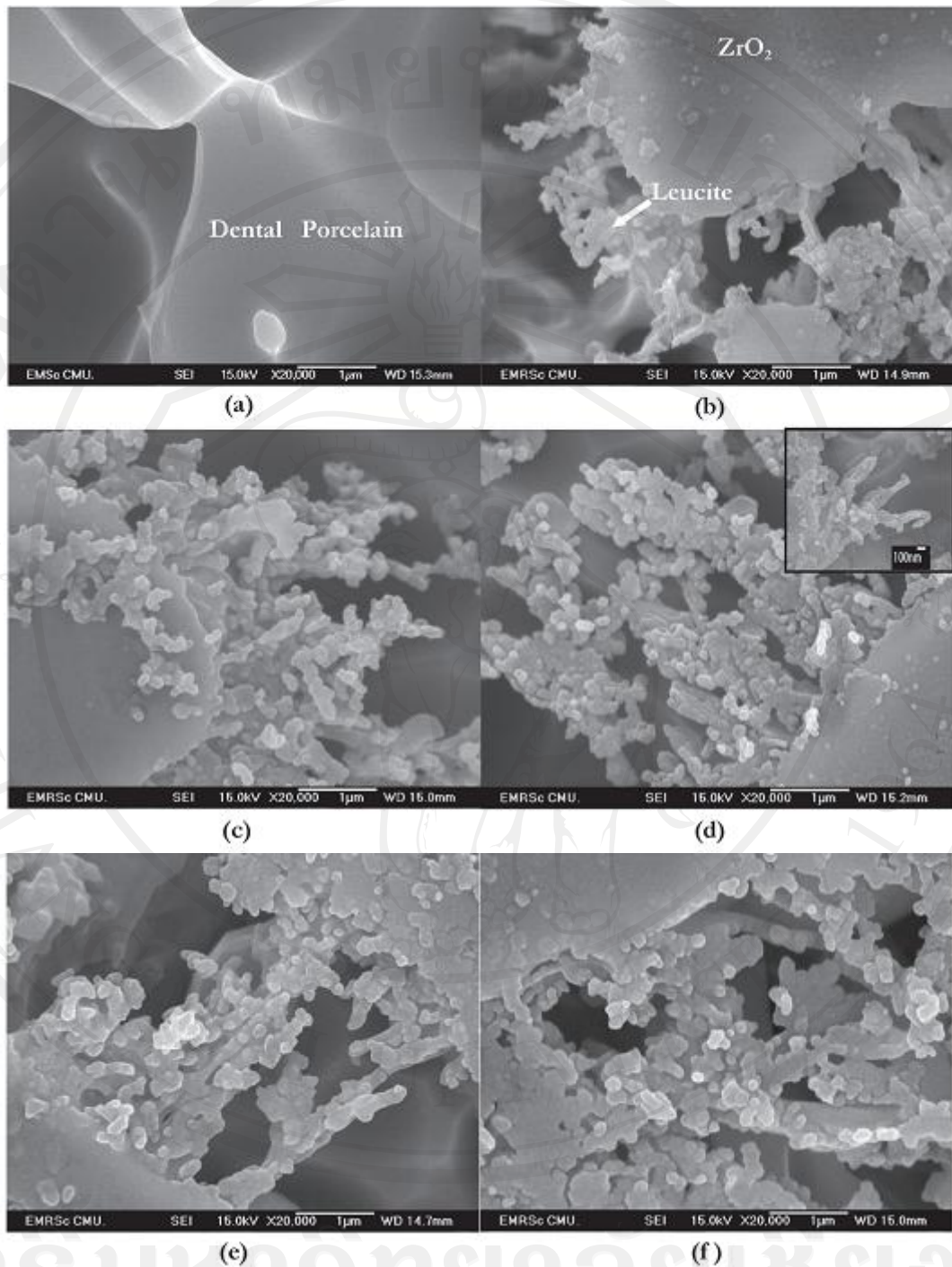
Fig. 4.3 SEM micrograph of (a) dental porcelain, (b) CG, (c) G5, (d) G6, (e) G7 and (f) G8 samples.
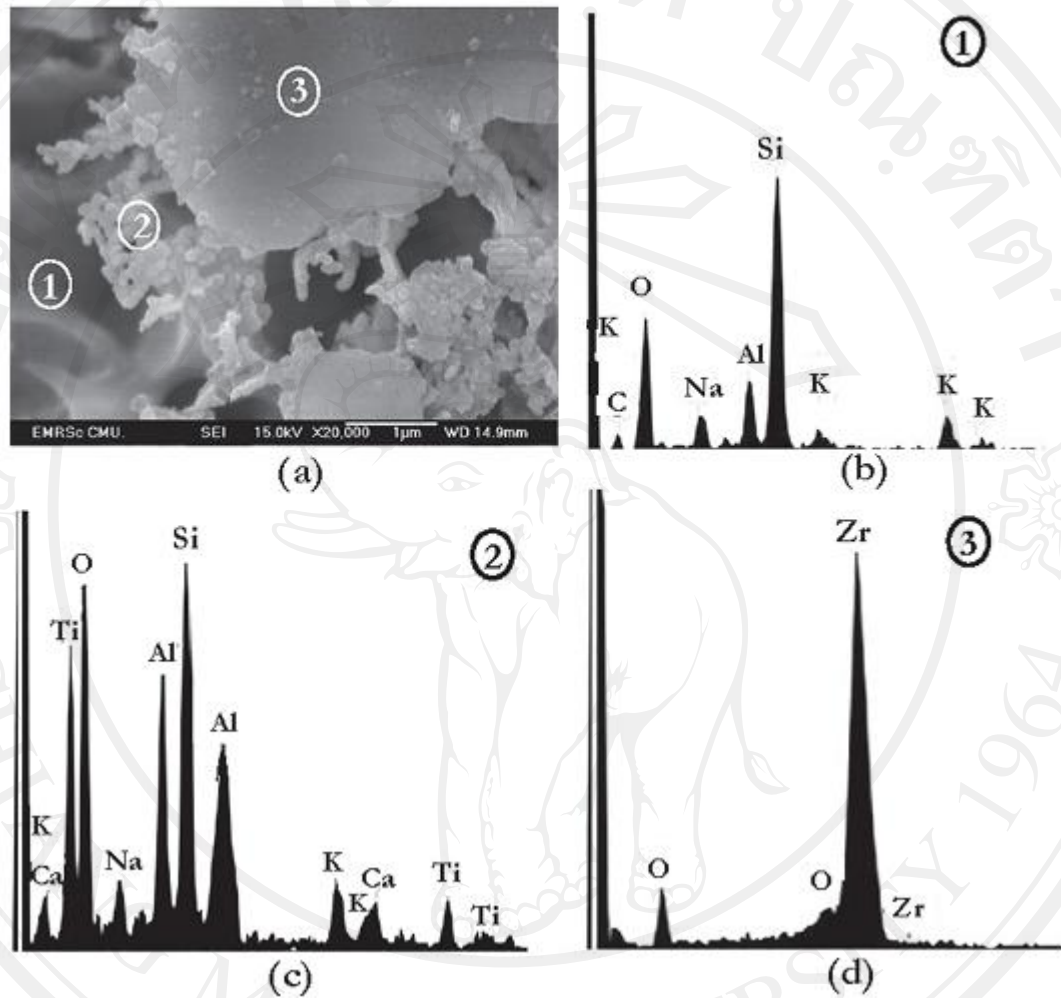
Fig. 4.4 Representative (a) SEM micrograph of CG samples and their corresponding EDX analysis, indicating the chemical compositions of (b) glassy matrix, (c) leucite and (d) ZrO_2 phases, respectively.

4.2 Mechanical properties

4.2.1 Hardness

Effect of tempering time on mechanical properties of each samples are given in Table 4.2, along with corresponding standard deviation. The hardness values of 20wt% ZrO_2 reinforced dental porcelain groups are greater than dental porcelain. Especially the two-step sintering groups show greater hardness more than CG.

Table 4.2 Average (and standard deviation) of the mechanical properties of ZrO_2-reinforced porcelain ceramics.

| Materials	Flexural strength (MPa)	Fracture toughness (MPa·m$^{1/2}$)	Elastic modulus (GPa)	Hardness (GPa)
Dental porcelain	82.27 (5.09)[a]	1.01 (0.10) [a]	58 (6.6)	4.93 (0.95) [a]
CG	83.48 (7.99) [a]	1.40 (0.24) [b]	101.33	5.26 (1.31) [a]
G5	83.50 (10.64) [a]	1.52 (0.26) [b]	101.33	4.96 (0.81) [a]
G6	84.42 (6.84) [a]	1.70 (0.26) [b]	101.33	5.53 (1.59) [a]
G7	83.43 (6.85) [a]	1.66 (0.59) [b]	101.33	5.05 (0.60) [a]
G8	83.21 (7.94) [a]	1.59 (0.04) [b]	101.33	4.98 (0.35) [a]

[a-b] There is no significant statistical different ($p > 0.05$) between materials with the same superscript letters.

65

The maximum of hardness is seen in G6 (5.53 GPa). In the tempering time range 0-30 min, the density increasing with increasing time. The present study found that the maximum density (2.76 g/cm^3) and hardness (5.53 GPa) were seen in G6. These results are in agreement with other works [161, 162] that stated the density and porosity affect the mechanical properties of dental porcelain. The increasing hardness can be attributed to the apparent decreased porosity and increase density of porcelain specimens. Consequently, less porosity and increased density values contributed higher hardness and flexural strength values. However, the hardness values of present study demonstrates that there is no statistically significant difference among them

The cracks produced with the indenter are symmetric (Fig. 4.5). Cracks in the dental porcelain ceramics propagated directly through the glassy phase (Fig. 4.6). Indentations of all ZrO$_2$-reinforced porcelain ceramics show asymmetric cracks (Fig. 4.7). The cracks pattern is consistently to the transgranular for zirconia grains, where as it is mainly intergranular for zirconia grains, excepted when the crack tip propagates perpendicularly to transverse grains (Fig. 4.8). SEM micrograph shows evidence of crack deflection and crack shielding (bridging and pull-out of the reinforcing and microcrack toughening (Fig. 4.8).
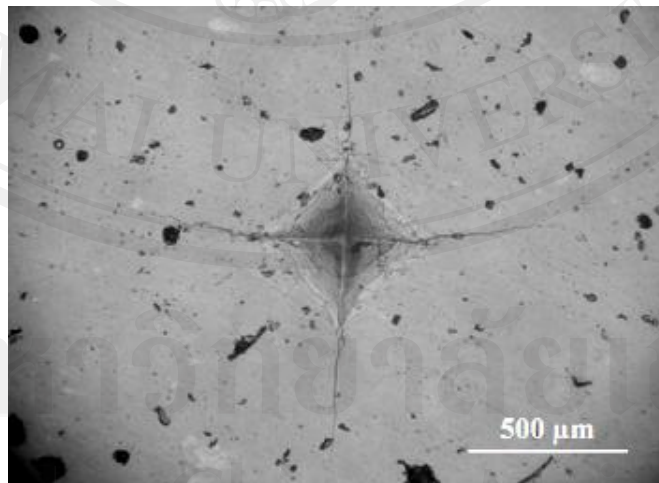

Fig. 4.5 Impression of a Vickers indenter producing symmetric cracks, where the cracks are propagating along the glassy phase of the matrix. The crack patterns are propagating normally to the orientation of the crystalline reinforced phase.
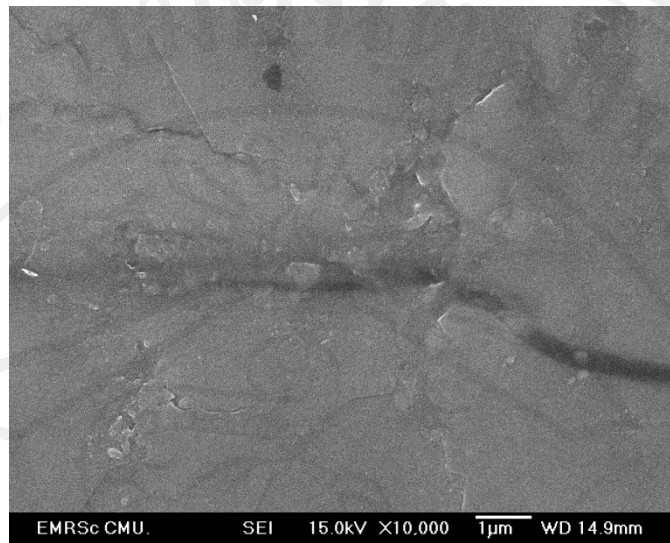
Fig. 4.6 SEM micrograph of cracks in the dental porcelain ceramics propagated directly through the glassy phase.
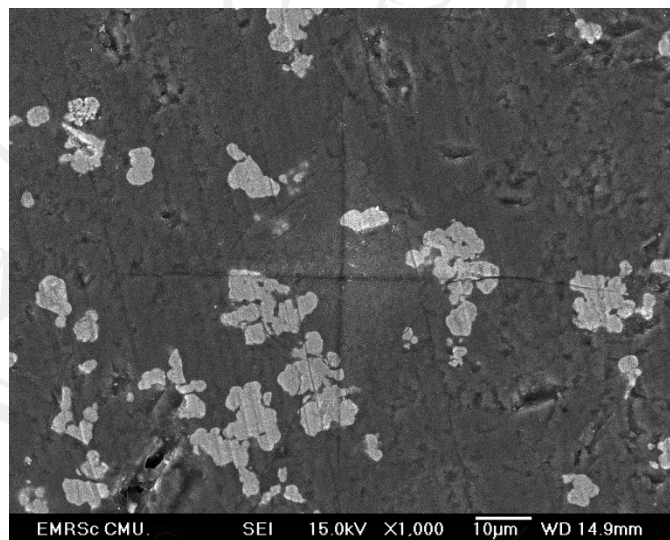
Fig. 4.7 Impression of a Vickers indenter producing symmetric cracks, where the cracks are propagating along the glassy phase of the matrix and crystalline reinforced phase.

(a)   (b)
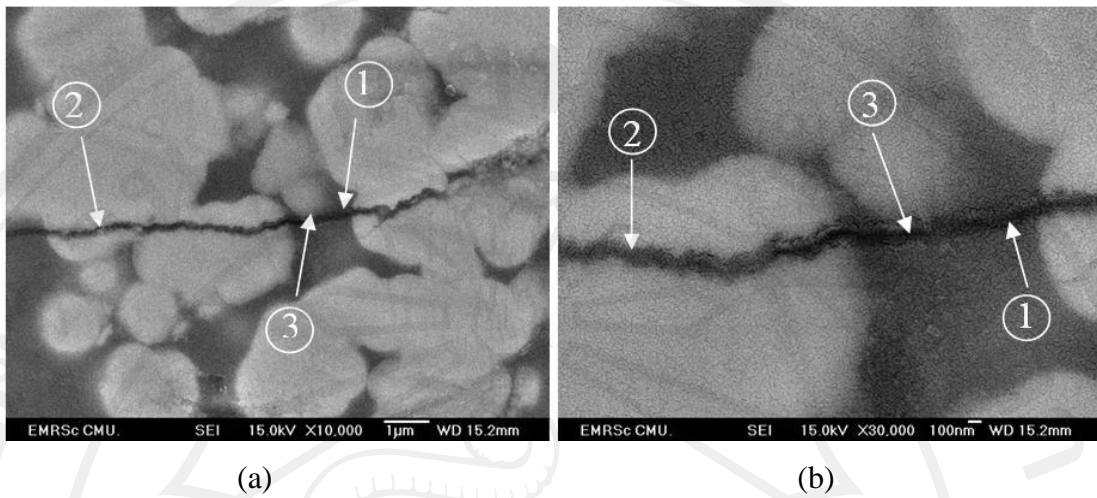
Fig. 4.8 SEM micrograph of (a) and (b) G6; (1) a branch of the intergranular crack is propagating through a glassy phase, (2) transgranular cracking through the grain of crystalline reinforced phase and (3) microcracks are visible in the glassy matrix and at the interface between particles and glass.

The common feature of dental porcelains is a considerable crystalline phase in the glassy matrix that results in a substantial contribution to the physical, optical, and mechanical properties and can affect toughness of the resulting composite ceramic. The size, distribution, and nature of the crystalline phases in dental ceramics appear to contribute most to the fracture behavior of the ceramic materials. Differences in thermal expansion coefficients among various phases can lead to localized stresses at phase boundaries and affect mechanical properties [161].

Mismatches between the thermal expansion coefficient the crystalline phase and glassy matrix can create boundary stresses during cooling. Morena et al. [163] observed in conventional high-expansion feldspathic porcelains at indentation cracks were deflected away from leucite crystals and consequently favored the glassy matrix for propagation. Presumably this response occurred because of interfacial stresses caused by a large thermal expansion mismatch between the leucite and glassy matrix and may account for the slightly greater fracture toughness measured in these materials over the glass control. Conversely, development of such localized residual stress fields has been implicated as a mechanism to improve toughness of the material

[164]. These localized residual stresses that are developed throughout the material can shield the crack by countering tensile forces, which drive the crack forward. The higher containing leucite-reinforced porcelains are likely to rely on this strengthening mechanism. The high coefficient of thermal contraction and volume reduction associated with the high-to-low temperature phase transformation of leucite created a situation that caused leucite crystals to contract substantially more than the glass matrix. Compressive forces are created in the glass matrix that surround the particle and are frozen during the cooling phase, whereas tensile forces are created in the particles, leading to microcracking in the leucite phase. The residual compressive stresses in the glass phase around the particles can counter tensile stresses that drive the crack forward [161].

The last remarkable, for the comparative all hardness in this chapter can be summarized in Fig. 4.9.

Hardness of ZrO_2-reinforced ceramics
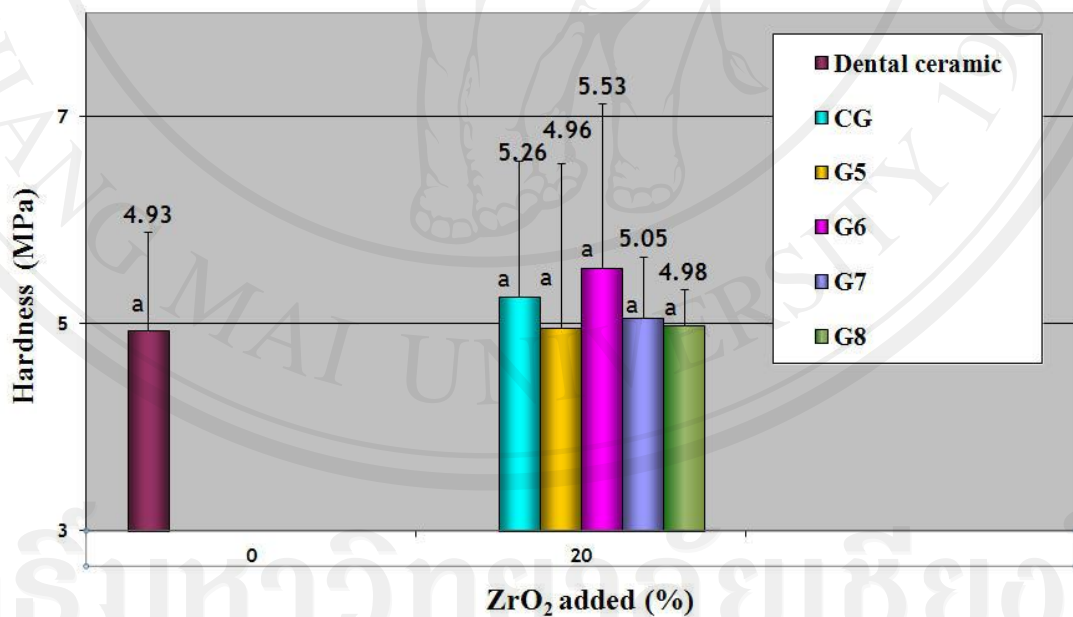
Fig. 4.9 The comparative all hardness data of ZrO_2-reinforced porcelain ceramics.
[a] There is no significant statistical different ($p > 0.05$) between materials with the same superscript letters.

4.2.2 Flexural strength

Flexural strength of dental porcelain in this study is 82.27 MPa (Table 4.2). This present study clearly indicated that values higher than those of specifications required by ISO 6872 [142], in agreement with other works [2, 3, 162]. The nanocomposite, increasing leucite content and density following tempering effect (G6-G8) were thought to be responsible for the increase in flexural strength [6, 162]. Leucite content was significantly higher after second sintering. The increase in leucite after firing is consistent with increase in flexural strength following firing observed by Dong et al. [31]. Maximum flexural strength values of 84.42 MPa were found in G6, while dental porcelain showed lowest flexural strength. Although the flexural strengths of G5-G8 have higher values than pure dental porcelain and CG, there is no statistically significance between them ($p > 0.05$). In fact there is no significant linear relationship between increasing addition of leucite and higher mean uniaxial flexural strength values that have been shown in this study and previous studies [6, 76, 87]. Although the inclusion of fine rather than larger particle sizes into a glassy matrix have produced minimal microcracking and flexural strength improvements in dental porcelain [34] but uniform distribution of leucite particles in the glassy matrix improve flexural strength. Literatures [6, 31] reported that the flexural strength of dental porcelain increased during heat pressing and further increased with the firing treatments required to produce the final restoration. They showed that the heat-pressing treatment produced better dispersion of fine leucite particles in the glassy matrix and attributed the improve strength following pressing to this better leucite dispersion

The flexural strength results of the Weibull analysis are presented in Table 4.3, together with the Weibull plots (Fig. 4.10 and 4.11). High Weibull moduli (steeper lines) indicated more uniform strength. Only CG and G6 showed good correlations with the regression used, according to the values of the 90% critical correlation coefficient (r). The statistical significance between the strength of materials tends towards that obtained by one-way ANOVA, where data sets were compared for the overlap of their double-sided confidence intervals at the 95% level. The high Weibull modulus for Dental porcelain, CG, G6, G7 and G8 indicated a uniform material with

reliable strength values. On the other hand, G5 had wide range of strength values with lower Weibull moduli.

The last remarkable, for the comparative all flexural strength in this chapter can be summarized in Fig. 4.12.
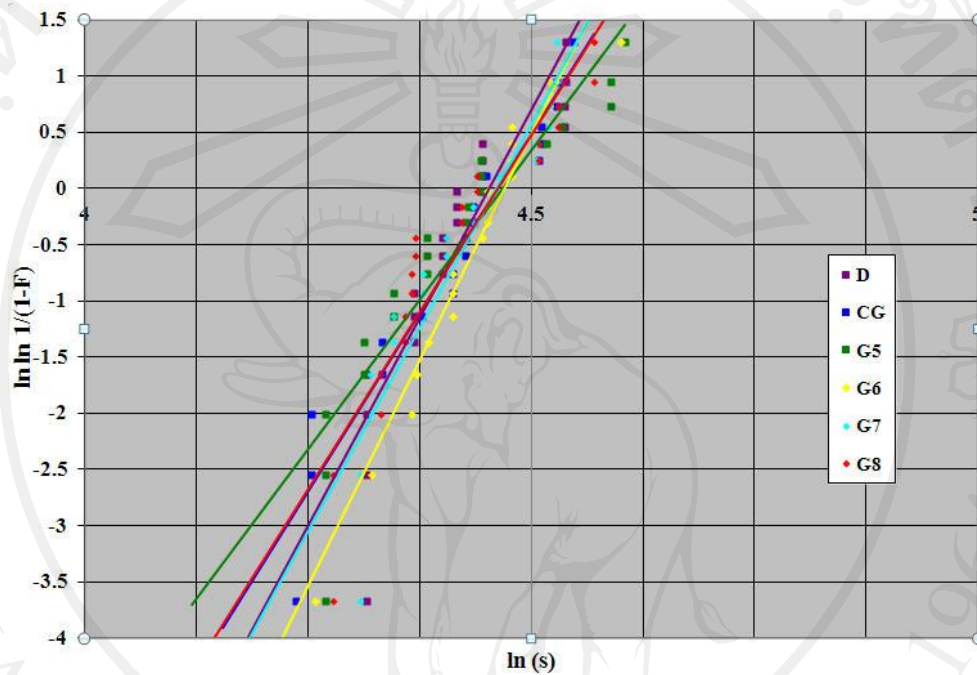
Fig. 4.10 Weibull plots of uniaxial flexure strength data for ZrO_2-reinforced porcelain ceramics.

Table 4.3 Results of the Weibull regression analysis of ZrO_2-reinforced porcelain ceramics.

| Materials	m Value	σ 0.01 (MPa)	σ 0.05 (MPa)	σ 0.10 (MPa)	r^2	$σ_0$	C.I. (95%) for $σ_0$
Dental porcelain	14.82	63.22	70.57	74.09	0.8235	82.49[a]	83.24-89.23
CG	12.69	60.17	68.42	72.41	0.9431	86.47[a]	82.86-90.08
G5	10.64	56.96	66.39	71.03	0.8363	87.76[a]	83.13-90.66
G6	16.09	66.10	73.15	76.30	0.9512	87.98[a]	85.02-90.95
G7	14.52	62.98	70.46	74.04	0.8739	86.45[a]	83.34-89.57
G8	12.60	60.44	68.78	72.83	0.8641	87.06[a]	83.45-90.66

[a] There is no significant Weibull statistical different ($p > 0.05$) between materials with the same superscript letters. m value is the Weibull modulus; σ 0.01, 0.05 and 0.10 is the stress levels at 1, 5 and 10% probability of failure, respectively; r^2 is the regression coefficient; $σ_0$ is the Weibull characteristic strength; C.I. is the confidence intervals.
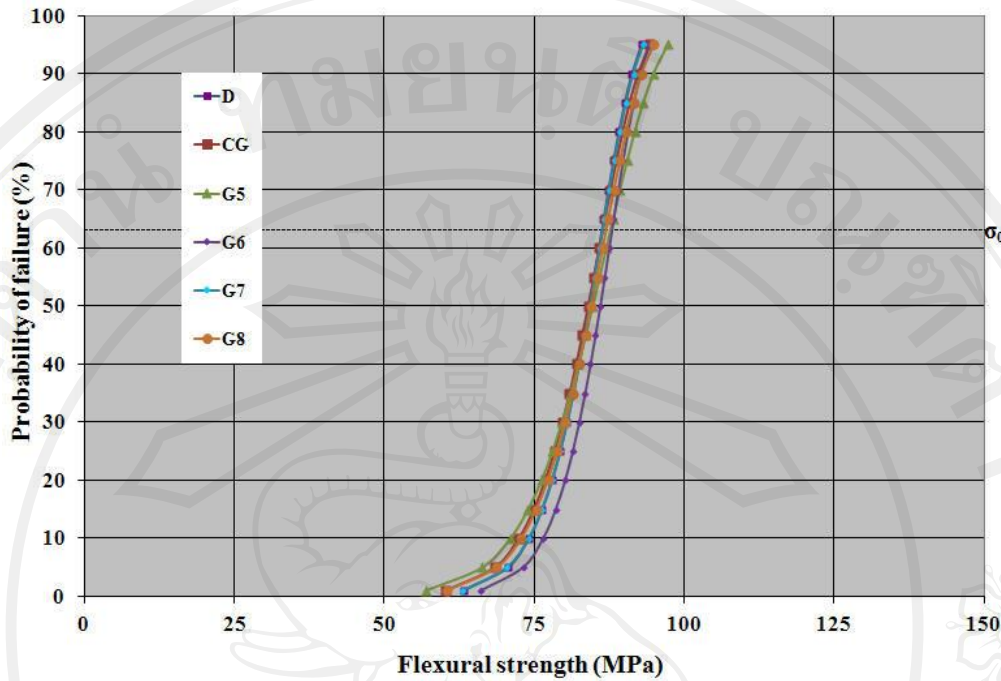
Fig. 4.11 The cumulative Weibull plots of probability of failure data for ZrO_2-reinforced porcelain ceramics.
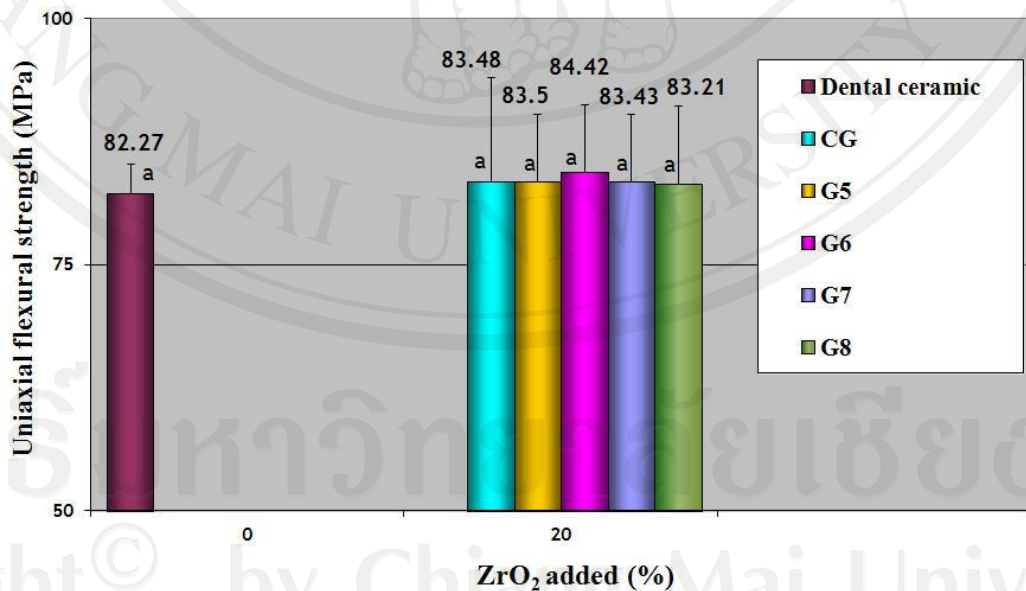
Fig. 4.12 The comparative all flexural strength data of ZrO_2-reinforced porcelain ceramics. [a] There is no significant statistical different ($p > 0.05$) between materials with the same superscript letters.
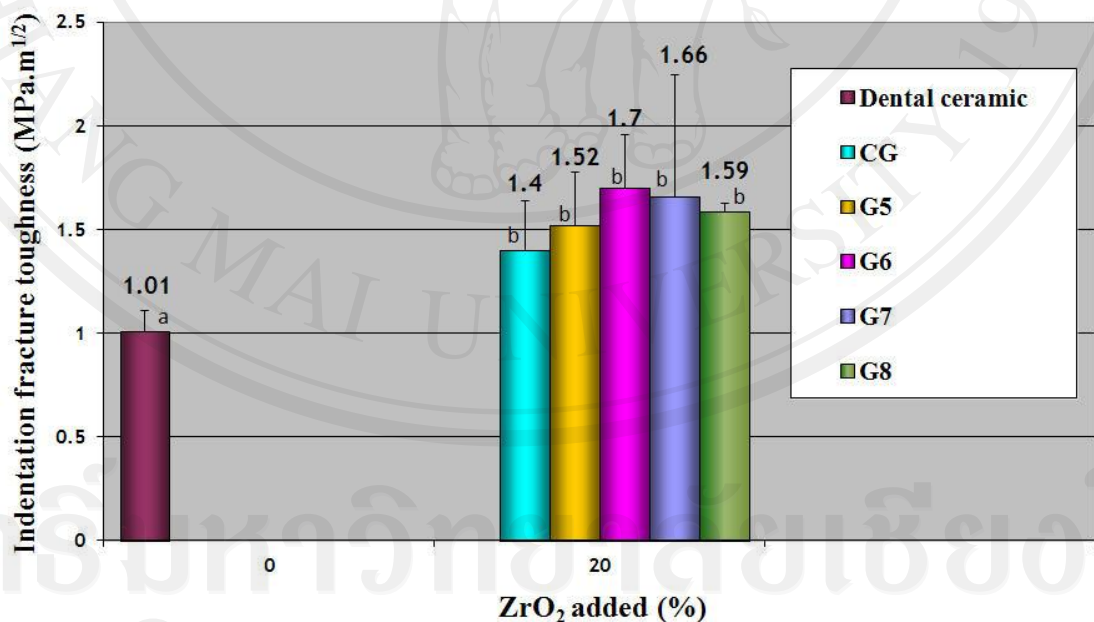
4.2.3 Fracture toughness

The fracture toughness results of this study are given in Table 4.2. The toughness of the dental porcelain (1.01 MPa.m$^{1/2}$) lies within the same range as observed by Craig and Powers [165]. Consistency with their reported data indicated the reliability of the indentation technique in evaluating the toughness of specimens. Brittle dental ceramics are incapable of absorbing appreciable amounts of elastic strain energy before fracture [163]. The resistance of a material to crack propagation is defined as fracture toughness and is one measure of the strain-energy-absorbing ability of brittle materials. The fracture toughness of a material is related to the tensile stress that must be achieved in a crack tip before fracture is initiated [166]. Therefore improved fracture toughness is a critical property to consider for selection of a dental ceramic restorative material. Although flexural strength of them is no significant statistical difference ($p \geq 0.05$), the fracture toughness values between dental porcelain and ZrO_2-reinforced porcelain ceramics are significant statistical difference ($p < 0.05$). These result is agreement with Segi et al [160] that found 18vol% Zirconia whiskers modify dental porcelain have greater fracture toughness than dental porcelain. The fracture toughness of all ZrO_2-reinforced porcelain ceramics was found to increase statistically significant compared with pure dental porcelain (Table 4.2). The toughness of all composite materials also exhibited a notable increasing. The higher toughness of all composite materials compared to dental porcelain is the result of the reinforcing second phase of zirconia and leucite [4-6]. Higher fracture toughness occurs oftener in two or more phase materials than in single-phase materials if the second reinforcing phase makes crack propagation more difficult, due to the formation of the crack requires higher energy [162]. The presence of rigid additives, zirconia reinforcing phase and especially the nanocomposite structure formations in these composite materials, contributed to the high toughness. The fracture toughness values of two-step sintering groups are greater than CG. There is no statistical significantly tougher ($p \geq 0.05$) among tempering time, however, the maximum of fracture toughness is seen in G6 (1.7 MPa·m$^{1/2}$) and the minimum of toughness is seen in CG (1.4 MPa·m$^{1/2}$). In contrast, Huang et al [167] reported that two-step sintering method influenced the sintering

property and mechanical properties of zirconia ceramic. They designed to use temperature of T_2 as half as it of T_1. The success of this two-step sintering may strongly depend on the choices of firing temperatures (T_1 and T_2). This section demonstrates that the strength of dental porcelain ceramics cannot be significantly enhanced by employing two-step sintering and the nanocomposite approach. The two-step sintering is aim to increase the density without obvious grain growth, to enhance mechanical properties [13]. The density and leucite particle size of one-step and two-step sintering groups in this study are not obvious difference. It can be explained that the nanocrystalline leucite cluster lack of uniform distribute, as explained in the topic 4.2.2. It can be concluded that the tempering time does not influence on mechanical properties ZrO_2-modified dental porcelain ceramics.

The last remarkable, for the comparative all fracture toughness in this chapter can be summarized in Fig. 4.13.

Fig. 4.13 The comparative all fracture toughness data of ZrO_2-reinforced porcelain ceramics.